Analysis of the contact interactions between fingertips and objects with different surface curvatures

J Z Wu* and **R G Dong**
National Institute for Occupational Safety and Health, Morgantown, West Virginia, USA

The manuscript was received on 3 February 2004 and was accepted after revision for publication on 6 December 2004.

DOI: 10.1243/095441105X9327

Abstract: Previous experimental observations indicated that the contact interactions between finger and tool handle interfere with the grasp stability, affecting the comfort and manipulations of hand-held tools. From a biomechanical point of view, the curvature of the contact surface should affect the contact pressure and contact area, and thereby the comfort and manipulations of hand tools. The current authors analysed, via a finite element model, the contact interactions between fingertips and objects with different curvatures. The effects of the curvature on the contact stiffness, fingertip deformations, contact pressure distributions, and stress/strain distributions within the soft tissues were analysed. The simulation results indicated that the curvature of the contact interface influences the contact characteristics significantly. For a given contact force, the contact area and the contact stiffness increase but the contact pressure and the fingertip deformation decrease with the decrease of the contact surface curvature. The present simulation results will be useful for ergonomic designers in their aim to improve the design of tool handles.

Keywords: computer simulations, fingertip, finite element analysis, grasp, soft tissue mechanics

1 INTRODUCTION

Nearly one million American workers each year report taking time away from work to treat and recover from musculoskeletal disorders [1]. Hand discomfort, especially carpal tunnel syndrome, tendinitis, and hand–wrist arthritis, accounts for a great portion of the total number of the musculoskeletal disorders. Approximately 1.87 million workers reported having carpal tunnel syndrome [2, 3], approximately 588 000 reported having tendinitis or related syndromes [3], and almost two million active or recent workers were estimated to have hand–wrist arthritis [3]. Almost all of these hand discomforts were among the workers using some kind of hand or power tools. For any tools from office equipment to heavy-duty construction power tools, handles serve as an interface between operators and machines. The contact interactions between hands and handles may interfere with manipulations and musculoskeletal loading during operations.

A tool handle designed to reduce fatigue and to improve comfort will lead to a reduction of musculoskeletal disorders in the hand. Grant *et al.* [4] and Kong and Freivalds [5] found that the grip strength depends strongly on the handle diameter, and the grip effort and the injury potential can be reduced by using handles of suitable diameter. Wu [6] and Chan [7] studied the effects of the handle diameter of chopsticks on the food-serving performance and found that the diameter of the chopsticks significantly influenced the food-pinching efficiency; the efforts of food-serving could be minimized using chopsticks with an optimized diameter (approximately 4–6 mm). The size of handles of power tools has been a major consideration for ergonomic designers in their aim to minimize the operation efforts and to maximize the gripping force and torque strength (e.g. see references [8–11]).

The contact interactions between finger and objects may interfere with grasp stability, thereby affecting the manipulations of hand-held tools. Jenmalm *et al.* [12] examined the influence of surface

* *Corresponding author: National Institute for Occupational Safety and Health, Morgantown, West Virginia, USA. email: jwu@cdc.gov*

were considered to be linearly elastic (Young's modulus = 200 GPa, Poisson's ratio = 0.3).

2.2 Numerical tests

In the simulations, the bone within the fingertip was considered to be fixed, while the contact object was subjected to a displacement towards the fingertip. The time history of the prescribed displacement was assumed to have a sinusoidal form with a changing speed, simulating the grasp task of the human hand [**21**]. The contact between the skin and curved contact surface was considered to be frictionless. The effects of material inertia and friction on contact pressure distributions were neglected. The force responses, the fingertip deformations, the contact pressure distributions, and the distributions of the stress/strain within the soft tissues, as a function of deformations, were calculated in the simulations.

A total of nine numerical tests of the contact interactions between a fingertip and contact surfaces with different curvatures were performed. In these tests, the dimensions of the fingertip were kept unchanged, while the curvature of the contact surfaces was varied in these nine simulation cases, i.e. convex with a radius of $R = 12$, 25, 50, and 100 mm; flat (i.e. $R \rightarrow \infty$); and concave with a radius of $R = -12$, -25, -50, and -100 mm, as shown in Fig. 2. By defining the concave contact surfaces and the convex contact surfaces using negative and positive radius respectively, the curvatures ($\kappa = 1/r$) of the contact surfaces simulated in the study are in a range from -0.083 to $+0.083\ \text{mm}^{-1}$.

3 RESULTS

In order to validate the proposed FE finger model, the numerical simulations on the contact interactions between a fingertip and a flat surface are compared with the published experimental data [**16**]. The normalized force response of the fingertip

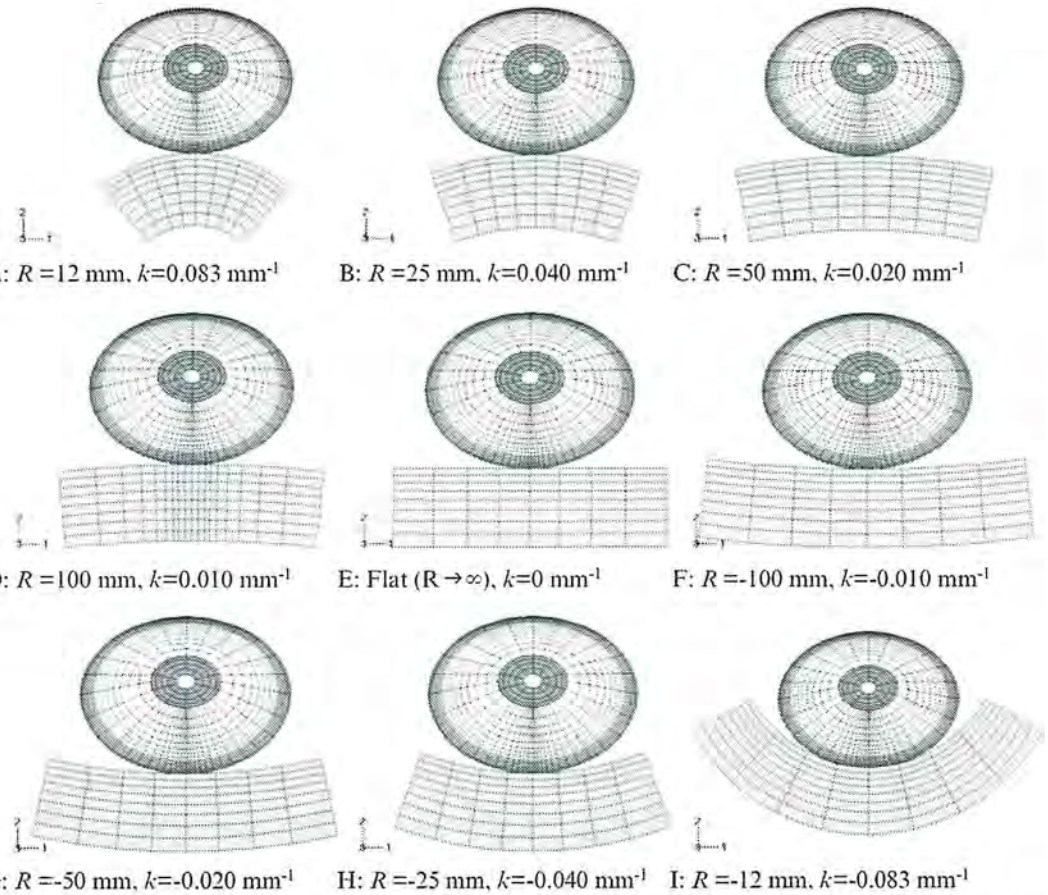

Fig. 2 Finite element models of the contact interactions between the fingertip and the contact surfaces of different curvatures. The contact between the fingertip and the contact surface was considered to be frictionless. The contact surface was assumed to be of steel (Young's modulus = 200 GPa, Poisson's ratio = 0.3). Numerical simulations were performed using nine different curvatures (κ) for the contact surface, as shown in the figure from (a) to (i)

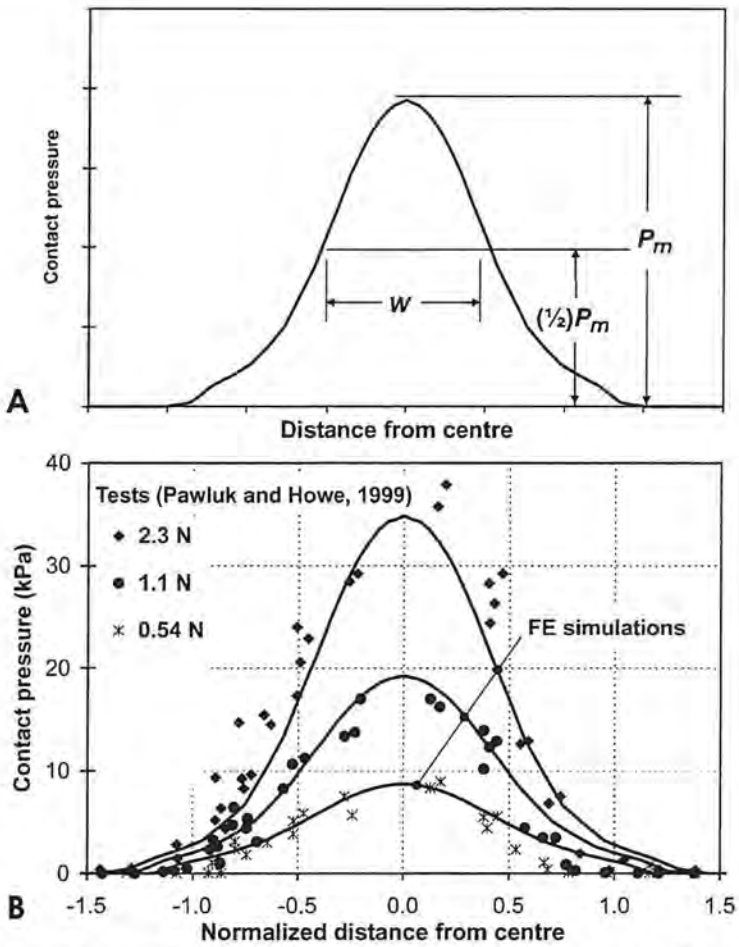

Fig. 4 Comparison of the contact pressure distributions at three force levels predicted using the current FE model with those obtained experimentally [**16**] for the contact between a fingertip and a flat surface. (a) Characteristic finger width, w, is defined as the contact pressure width at half of the maximum pressure values, p_m, for a contact force of 1 N. (b) Comparison of the predicted contact pressure distributions at three contact force levels (0.54, 1.1, and 2.3 N) with the experimental data [**16**]. The distance from the centre is normalized using the characteristic finger width, w, as defined in (a). A section thickness of 12 mm was used in the two-dimensional FE model to calculate the contact force

For all cases, the central contact pressure increases almost linearly with increasing contact force, as shown in Fig. 10(a). The slope of these curves decreases when the curvature of the contact plate varied from convex to concave. The central contact pressure is plotted as a function of the displacement of the contact plate for all simulated cases, as in Fig. 10(b). It is interesting to see that the relationship between the central contact pressure and the displacement is independent of the curvature of the contact surface.

The distributions of the horizontal (E_{11}) and vertical (E_{22}) strains within the soft tissues of the fingertip, which is in contact with a flat surface under three different loadings of 0.02, 0.04, and 0.08 N/mm, are shown in Figs 11(a), (b), and (c) respectively. It is seen that the strains within the soft tissues of the fingertip increase with the increased loading; the soft tissues undergo tensile straining in the horizontal directions (E_{11}) and compressive straining in the vertical directions (E_{22}).

The effects of the curvature of the contact plate on the distributions of the strains within the soft tissues of the fingertip are analysed by comparing the distributions of the horizontal (E_{11}) and vertical (E_{22}) strains within the soft tissues of the fingertip, which is in contact with contact surface of three different curvatures (convex with a radius of 25 mm, and flat and concave with a radius of -25 mm) while under the same loading (0.04 N/mm), as in Fig. 12. It is seen that the strains within the soft tissues of the fingertip depend on the curvature of the contact plate and

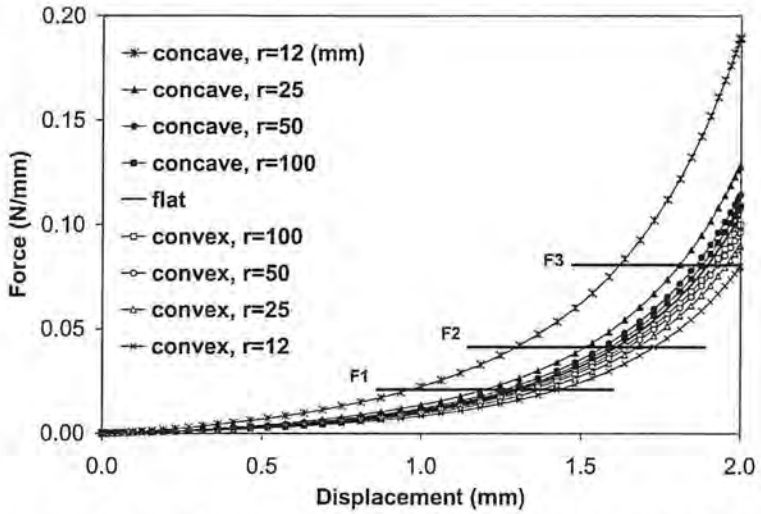

Fig. 6 The stiffness of the contact interactions between the fingertip and the contact surface of different curvatures. The contact stiffness increases with deceasing curvature of the contact surface. For the same loading (e.g. F_1, F_2, and F_3), the displacement for the contact interaction with a concave surface is smaller than that with a convex surface

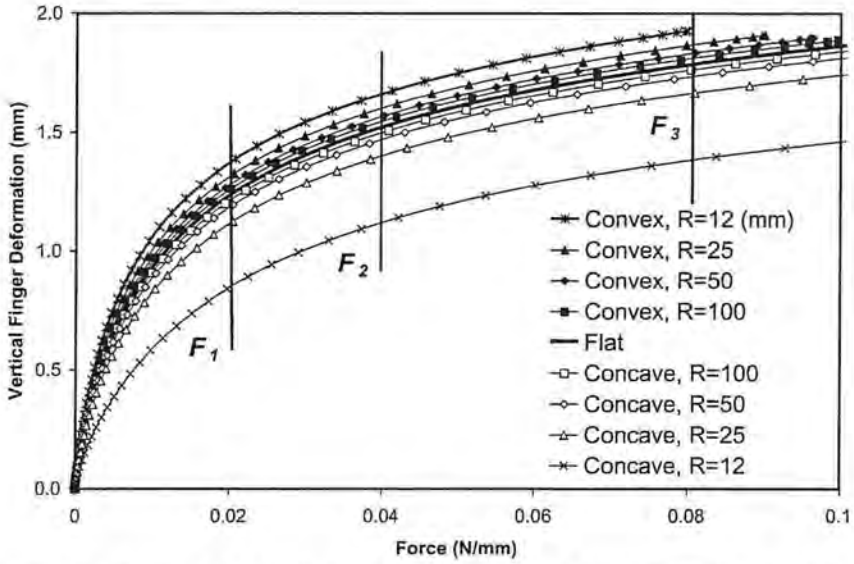

Fig. 7 The vertical fingertip deformation as a function of the contact force for the contact interactions with contact surfaces of different curvatures. The fingertip deformation decreases with decreasing curvature of the contact surface. For the same loading (e.g. F_1, F_2, and F_3), the fingertip deformation for the contact interaction with a concave surface is smaller than that with a convex surface. The vertical fingertip deformation is calculated by the difference in the displacements between the centre of the contact surface and the centre of the nail surface

white finger has been related to the high contact pressures at the fingertips [**22–24**]. The concentrated contact pressure at the fingertips under tool vibration is believed to affect the haemodynamic forces in the arterial walls and produces alteration of the arterial blood flow, thereby inducing degenerations of neural and vascular system in the fingers. Therefore, reducing the concentrations of contact pressure in the tool handle will not only help improve the comfort in tool manipulations but also reduce the risk of the hand–arm vibration syndrome.

The current simulation results indicated that the curvature of the contact interface significantly influences the contact characteristics. The stiffness of contact increased gradually when the contact surface curvature varied from 0.01 to $-0.04\ \text{mm}^{-1}$ (Figs 5 to 7). A further reduction of the contact surface curvature resulted in a rapid increase in the contact

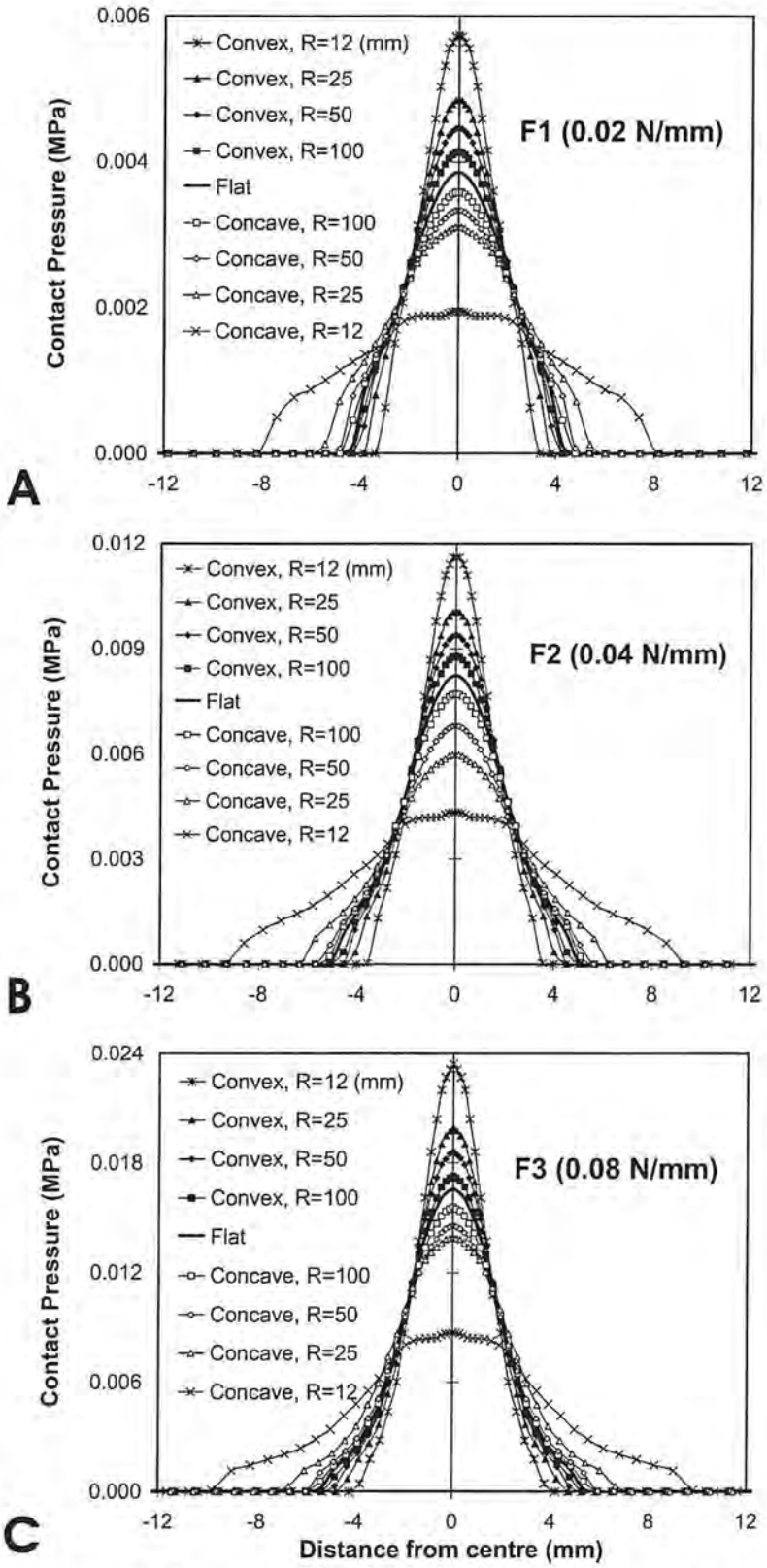

Fig. 9 Contact pressure distributions as a function of contact surface curvature for three different loading levels: (a) $F_1 = 0.02$ N/mm; (b) $F_2 = 0.04$ N/mm; (c) $F_3 = 0.08$ N/mm. The contact pressure and contact surface increase with increasing contact surface curvature

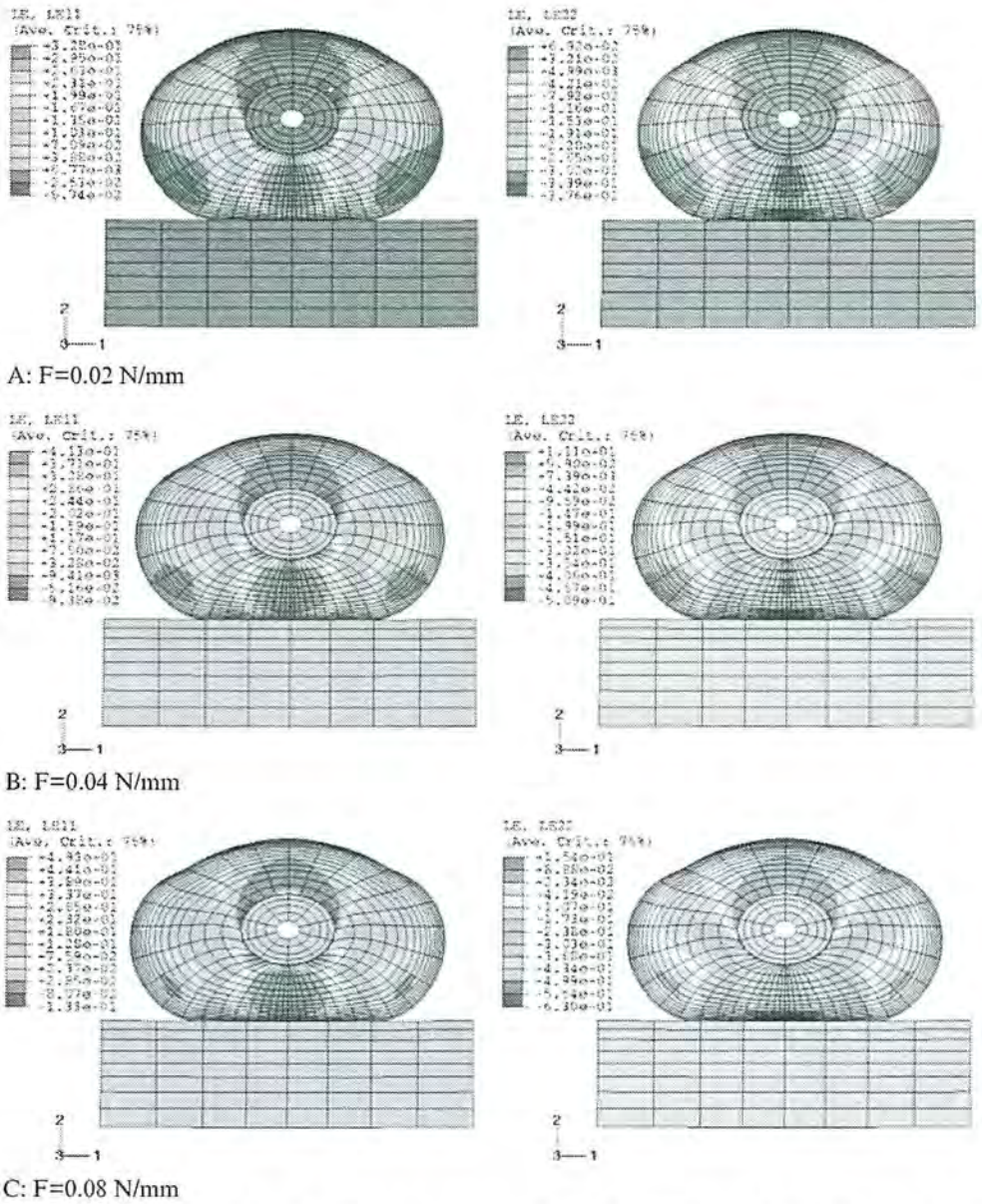

Fig. 11 Deformation and strain distributions within the soft tissues of the fingertip in contact with a flat surface under three different loading levels: (a) $F_1 = 0.02$ N/mm; (b) $F_2 = 0.04$ N/mm; (c) $F_3 = 0.08$ N/mm. The figures in the left column are the strain distributions in the horizontal direction (E_{11}), while those in the right column are the strain distributions in the vertical direction (E_{22})

the thickness and properties of the covering materials.

The numerical simulations conducted in the present studies were based on a two-dimensional FE model that is different from real, three-dimensional cases where many tool handles have a curvature that is not constant but varies as a function of length. Therefore, the absolute values of the contact stiffness, contact pressures, and stresses in the soft tissues may be different from the real cases. However, the trends of the effects of the curvature of the contact surfaces predicted here using the two-dimensional model should be reasonable.

In summary, the contact interactions between the fingertips and objects with different curvatures have been analysed via a finite element model in the present study. The curvature of the contact surface has been found to affect the contact stiffness, fingertip deformations, contact pressure distributions, and stress/strain distributions within the soft tissues. The present simulation results will be useful to ergonomic designers in improving the design of tool

5 **Kong, Y. K.** and **Freivalds, A.** Evaluation of meathook handle shapes. *Int. J. Ind. Ergon*, 2003, **32**, 13–23.
6 **Wu, S. P.** Effects of the handle diameter and tip angle of chopsticks on the food-serving performance of male subjects. *Appl. Ergon*, 1995, **26**(6), 379–385.
7 **Chan, T.** A study for determining the optimum diameter of chopsticks. *Int. J. Ergon*, 1999, **23**, 101–105.
8 **Adams, S. K.** and **Peterson, P. J.** Maximum voluntary hand grip torque for circular electrical connectors. *Appl. Ergon*, 1990, **21**, 78–79.
9 **Bjoring, G., Johansson, L.,** and **Hagg, G.** Choice of handle characteristics for pistol grip power tools. *Int. J. Ergon*, 1999, **24**, 647–656.
10 **Imrhan, S. N.** and **Sundararajan, K.** An investigation of finger pull strengths. *Ergon*, 1992, **35**(3), 289–299.
11 **Imrhan, S. N.** and **Farahmand, K.** Male torque strength in simulated oil rig tasks: the effects of grease-smeared gloves and handle length, diameter and orientation. *Appl. Ergon*, 1999, **30**, 455–462.
12 **Jenmalm, P., Goodwin, A. W.,** and **Johansson, R. S.** Control of grasp stability when humans lift objects with different surface curvatures. *J. Neurophysiol.*, 1998, **79**(4), 1643–1652.
13 **Freund, J., Toivonen, R.,** and **Takala, E. P.** Grip forces of the fingertips. *Clin. Biomechanics* (Bristol, Avon), 2002, **17**(7), 515–520.
14 **Oh, S.** and **Radwin, R. G.** Pistol grip power tool handle and trigger size effects on grip exertions and operator preference. *Human Factors*, 1993, **35**(3), 551–569.
15 **Serina, E., Mote, C.,** and **Rempel, D.** Force response of the fingertip pulp to repeated compression – effects of loading rate, loading angle and anthropometry. *J. Biomechanics*, 1997, **30**(10), 1035–1040.
16 **Pawluk, D.** and **Howe, R.** Dynamic contact of the human fingerpad against a flat surface. *Trans. ASME, J. Biomech. Engng*, 1999, **121**(6), 605–611.
17 **Wu, J. Z., Dong, R. G., Smutz, W. P.,** and **Rakheja, S.** Dynamic interaction between a fingerpad and a flat surface: experiments and analysis. *Med. Engng Physics*, 2003, **25**(5), 397–406.
18 **Wu, J. Z., Dong, R. G., Smutz, W. P.,** and **Schopper, A. W.** Modeling of time-dependent force response of fingertip to dynamic loading. *J. Biomechanics*, 2003, **36**, 383–392.
19 **Wu, J. Z., Dong, R. G., Schopper, A. W.,** and **Smutz, W. P.** Analysis of skin deformation profiles during sinusoidal vibration of fingerpad. *Ann. Biomed. Engng*, 2003, **31**(7), 867–878.
20 **Clemente, C. D.** *Anatomy: A Regional Atlas of the Human Body*, 2nd edition, 1981 (Urban and Achwarzengerg, Baltimore and Munich).
21 **Rempel, D., Dennerlein, J., Mote Jr, C.,** and **Armstrong, T.** A method of measuring fingertip loading during keyboard use. *J. Biomechanics*, 1994, **27**, 1101–1104.
22 **Nerem, R.** Vibration enhancement of blood–arterial wall macromolecule transport. In International Hand–Arm Vibration Conference, Cincinnati, USA, 1977, pp. 37–41.
23 **Bovenzi, M.** Vibration white finger, digital blood pressure, and some biochemical findings on workers operating vibrating tools in the engine manufacturing industry. *Am. J. Ind. Medicine*, 1988, **14**(5), 575–584.
24 **Ekenvall, L.** and **Lindblad, L. E.** Vibration white finger and digital systolic pressure during cooling. *Br. J. Ind. Medicine*, 1986, **43**(4), 280–283.
25 **Tschoegl, N. W.** *The Phenomenological Theory of Linear Viscoelastic Behavior: An Introduction*, 1989 (Springer-Verlag, New York).
26 **Storakers, B.** On material representation and constitutive branching in finite compressible elasticity. *J. Mech. Phys. Solid*, 1986, **34**(2), 125–145.
27 **Mow, V. C., Kuei, S. C., Lai, W. M.,** and **Armstrong, C. G.** Biphasic creep and stress relaxation of articular cartilage: theory and experiment. *Trans. ASME, J. Biomech. Engng*, 1980, **102**, 73–84.
28 **Homes, M.** and **Mow, V. C.** Nonlinear characteristics of soft gels and hydrated connective tissues in ultrafiltration. *J. Biomechanics*, 1990, **23**, 1145–1156.
29 **Wu, J. Z.** and **Herzog, W.** Finite element simulation of location- and time-dependent mechanical behavior of chondrocytes in unconfined compression tests. *Ann. Biomed. Engng*, 2000, **28**(3), 318–330.
30 **Yamada, H.** *Strength of Biological Materials*, 1970 (Williams and Wilkins, Baltimore, Maryland).
31 **Pan, L., Zan, L.,** and **Foster, F.** Ultrasonic and viscoelastic properties of skin under transverse mechanical stress *in vitro*. *Ultrasound Med. Biology*, 1998, **24**(7), 995–1007.
32 **Wan Abas, W. A.** Biaxial tension test of human skin *in vivo*. *Biomed. Mater. Engng*, 1994, **4**(7), 473–486.
33 **Zheng, Y. P.** and **Mak, A. F.** An ultrasound indentation system for biomechanical properties assessment of soft tissues *in vivo*. *IEEE Biomed. Engng*, 1996, **43**(9), 912–918.
34 **Zhang, J., Mak, A.,** and **Huang, L.** A large deformation biomechanical model for pressure ulcers. *Trans. ASME, J. Biomech. Engng*, 1997, **119**, 406–408.

APPENDIX 1

Notation

$\bar{C}$	right Cauchy–Green deformation tensor
e	void ratio at the deformed state
e_0	void ratio at the undeformed state
E_{11} and E_{22}	horizontal and vertical strains respectively
F_1, F_2, and F_3	constant forces applied on finger
$\bar{F}$	deformation gradient tensor

the solid and fluid phases, $\bar{\sigma}^s$ and $\bar{\sigma}^f$ respectively

$$\begin{aligned}\tilde{\sigma}^t &= \tilde{\sigma}^f + \tilde{\sigma}^s \\ \tilde{\sigma}^f &= -\Phi^f p\mathbf{I} \\ \tilde{\sigma}^s &= \tilde{\sigma}^s_0 - \Phi^s p\mathbf{I}\end{aligned} \tag{5}$$

where Φ^s and Φ^f, with $\Phi^s + \Phi^f = 1$, are the instantaneous volume fractions of the solid and fluid phases respectively; p is the fluid pressure; the superscripts s and f imply the solid and fluid phases respectively. The stress in solid, $\bar{\sigma}^s$, is determined using equations (3) and (4).

The equation of motion of the tissue is governed by

$$\nabla \cdot \tilde{\sigma}^s + \tilde{\pi}^s = 0, \qquad \nabla \cdot \tilde{\sigma}^f + \tilde{\pi}^f = 0 \tag{6}$$

where $\bar{\pi}^f$ and $\bar{\pi}^s$ are the momentum exchanges, given by

$$\tilde{\pi}^f = -\tilde{\pi}^s = \Phi^s \nabla p + K(\tilde{v}^s - \tilde{v}^f) \tag{7}$$

where $\bar{v}^f$ and $\bar{v}^s$ are the speed of the fluid and solid phases respectively, K is the diffusive drag constant, which measures the frictional resistance of the fluid flowing through the solid matrix and is related to the hydraulic permeability, k, by $K = (\Phi^f)^2/k$. The hydraulic permeability is considered to be deformation-dependent [**28**, **29**]

$$k = k_0 \left(\frac{e}{e_0}\right)^n \exp\left\{\frac{M}{2}\left[\left(\frac{1+e}{1+e_0}\right)^2 - 1\right]\right\} \tag{8}$$

where e and e_0 are the void ratios at the deformed and undeformed states respectively, k and k_0 are the hydraulic permeabilities at the deformed and undeformed state respectively, and M and n are the material parameters.

APPENDIX 3

The Young's moduli of the bone and nail were assumed, according to the published experimental data [**30**], to be 17.0 GPa and 170.0 MPa respectively, while Poisson's ratio was assumed to be 0.30 for both. The material parameters of the skin and subcutaneous tissues used in the present simulations were determined based on published experimental data [**31–33**] (see Tables 1 to 3). The hydraulic permeability of the soft tissue has not been measured experimentally to date. It has been assumed that the permeability of the soft tissue is similar to that of articular cartilage [**28**], as suggested by Zhang *et al.* [**34**].

Table 1 Material parameters characterizing hyperelasticity and viscoelasticity for the skin ($\nu = 0.40$)

	i		
	1	2	3
α_i	4.941	6.425	4.712
μ_i (MPa)	-7.594×10^{-2}	1.138×10^{-2}	6.572×10^{-2}
g_i	0.148	0.252	–
τ_i (s)	2.123	9.371	–

Table 2 Material parameters characterizing the hyperelasticity for the subcutaneous tissue ($\nu = 0.40$)

	i		
	1	2	3
α_i	5.511	6.571	5.262
μ_i (MPa)	-4.895×10^{-2}	9.889×10^{-3}	3.964×10^{-2}

Table 3 Material parameters of hydraulic permeability for the subcutaneous tissue

M	n	k_0(m^4/N s)	e_0
4.638	0.0848	1.0×10^{-15}	1.5